BIOCHEMISTRY
including biophysical chemistry & molecular biology

Article

pubs.acs.org/biochemistry

Structural and Thermodynamic Characterization of Nore1-SARAH: A Small, Helical Module Important in Signal Transduction Networks

Cihan Makbul,[†] Diana Constantinescu Aruxandei,[†,⊥] Eckhard Hofmann,[‡] Daniel Schwarz,[§] Eva Wolf,[∥] and Christian Herrmann*[,†]

[†]Ruhr University, Department of Physical Chemistry I, Protein Interactions, Universitätsstrasse 150, 44780 Bochum, Germany

[‡]Ruhr University, Department of Biophysics, Protein Crystallography, Universitätsstrasse 150, 44780 Bochum, Germany

[§]Max Planck Institute of Molecular Physiology, Otto-Hahn-Strasse 11, 44227 Dortmund, Germany

[∥]Ludwig-Maximilians-University Munich, Department of Physiological Chemistry, Adolf Butenandt Institute, Butenandtstrasse 5, 81377 Munich, Germany

ABSTRACT: Tumor suppressor Nore1, its acronym coming from novel Ras effector, is one of the 10 members of the Rassf (Ras association domain family) protein family that have been identified. It is expressed as two mRNA splice variants, Nore1A and a shorter isoform, Nore1B. It forms homo- and heterocomplexes through its C-terminal SARAH (Sav/Rassf/Hpo) domain. The oligomeric state of Nore1 and other SARAH domain-containing proteins is important for their cellular activities. However, there are few experimental data addressing the structural and biophysical characterization of these domains. In this study, we show that the recombinant SARAH domain of Nore1 crystallizes as an antiparallel homodimer with representative characteristics of coiled coils. As is typical for coiled coils, the SARAH domain shows a heptad register, yet the heptad register is interrupted by two stutters. The comparisons of the heptad register of Nore1-SARAH with the primary structure of Rassf1−4, Rassf6, MST1, MST2, and WW45 indicate that these proteins have a heptad register interrupted by two stutters, too. Moreover, on the basis of the structure of Nore1-SARAH, we also generate structural models for Rassf1 and Rassf3. These models indicate that Rassf1- and Rassf3-SARAH form structures very similar to that of Nore1-SARAH. In addition, we show that, as we have previously found for MST1, the SARAH domain of Nore1 undergoes association-dependent folding. Nevertheless, the Nore1 homodimer has a lower affinity and thermodynamic stability than the MST1 homodimer, while the monomer is slightly more stable. Our experimental results along with our theoretical considerations indicate that the SARAH domain is merely a dimerization domain and that the differences between the individual sequences lead to different stabilities and affinities that might have an important functional role.

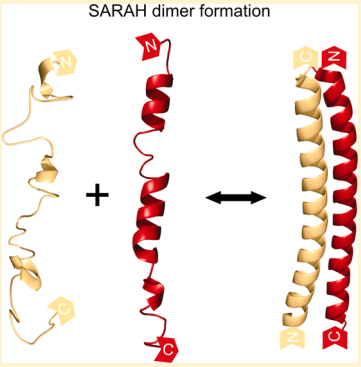

Rassf proteins are Ras effectors that interact with GTP-bound Ras (active form of Ras) through their Ras binding domain (RBD) and are supposed to act as tumor suppressors by regulating the cell cycle and apoptosis.[1−4] The best-characterized members of this family are Nore1 (also termed Rassf5) and Rassf1. Nore1 is expressed in two mRNA splice variants, Nore1A (413 residues) and the shorter variant, Nore1B (also termed RAPL, 265 residues). Nore1A has a broad spectrum of cellular activities and is widely expressed in comparison to Nore1B, which is located predominantly in lymphoid tissues. Nore1A is involved in the regulation of growth suppression,[5] apoptosis,[6,7] microtubule dynamics,[8,9] and cell cycle progression by delaying the transition from the S to the G_1 phase.[10,11] Nore1A is inactivated by hypermethylation of its promoter region in a large number of tumor cell lines.[12] In comparison, Nore1B is reported to be inactivated in only a small number of tumor cell lines. It participates in the regulation of cell adhesion and polarization of lymphocytes[13] and also functions in the microtubule dynamics of migrating cells.[14]

Nore1A has a proline rich domain at its N-terminus, followed by a C1 and Ras binding domain (RBD) and a C-terminal SARAH domain. Nore1B's RBD and SARAH domains are identical to those of Nore1A, but its N-terminus is divergent, consisting of a unique 40-amino acid sequence.

One of the most important properties of Nore1 is its ability to bind specifically with high affinity to the small GTPase Ras[15] as well as to mammalian Sterile20-like protein kinase 1 (MST1). The crystal structure of the Nore1−RBD−Ras complex shows that, compared to those of other Ras effectors, the contact area of Nore1 is extended, with additional structural elements forming a unique Ras switch II binding site. Thus, the Nore1−Ras complex is characterized by a small K_D value (0.08 μM) and a remarkably long lifetime (10 s) compared to those of other Ras effectors (0.1−1 s).[15] *Ras* and many of its other effectors like *Raf* encode proto-oncogenes whose protein

Received: October 27, 2012
Revised: December 28, 2012
Published: January 18, 2013

dx.doi.org/10.1021/bi3014642 | *Biochemistry* 2013, 52, 1045−1054

products show enzymatic activity.[16] In contrast to these proteins, Nore1 shows no enzymatic activity, and it was shown that it acts as a tumor suppressor protein triggering anti-oncogenic processes.[17] The treatment of cells with etoposide or exposure to UV irradiation can activate the S/T kinase MST1, which can induce apoptosis.[18] In this context, Nore1 probably relays signals coming from Ras to MST1 and plays a unique role (along with other Rassf members) among Ras effectors.[19] This suggests that Ras is involved not only in the regulation of processes triggering the development of cancer but also in that of opposite processes like cell cycle arrest and apoptosis, depending on the cellular context. By means of two-hybrid screens using a cDNA library of human lung and MST1 as bait, Rassf1−5 were identified as MST1 interacting partners.[7] It was demonstrated that MST1 specifically binds to Rassf1[20] and Nore1.[6] A direct interaction of MST1 and WW45 was also demonstrated.[21] The interaction between MST1 and Nore1 is mediated by their SARAH domains. To date, nine mammalian proteins were shown to contain a C-terminal SARAH domain, including MST1 and Nore1: Ras association domain family members 1−6 (Rassf1−6, respectively), MST1 and -2, and WW45 (ExPASy proteomics server of the Swiss Institute of Bioinformatics). Additionally, some of these proteins have isoforms with different lengths. Interestingly, the longer isoforms are widely expressed, whereas the shorter ones show pronounced tissue specificities.[22]

The central function of the SARAH domain seems to be the mediation of homo- and hetero-oligomerization between SARAH domain-containing proteins. For Nore1, Rassf1, and MST1, it was demonstrated that their SARAH domains are important for their diverse cellular functions.[6,7,20] The SARAH domains are approximately 50 amino acids long and seem to form multioligomeric structures[23] with coiled coil properties. However, apart from the results of Constantinescu Aruxandei et al.[24] and Hwang et al.,[25] there are few experimental data available in the literature about structural and biophysical characteristics of SARAH domains.

As the SARAH domain of Nore1 seems to be critical for its cellular activities, we focused our efforts on the structural and thermodynamic characterization of this domain. We were able to crystallize and determine the structure of the SARAH domain of murine Nore1. The primary structure of murine Nore1-SARAH differs from that of human Nore1-SARAH by three residues only. On the basis of this structure, we generated models for Rassf1-SARAH and Rassf3-SARAH that have sequences highly identical to that of Nore1-SARAH. Moreover, we compared the SARAH domain of Nore1 with that of other proteins to unveil general properties of this domain. Further, we investigated the thermodynamic stability of Nore1-SARAH by far-UV circular dichroism (CD) spectroscopy and isothermal titration calorimetry (ITC) and compared the results with those determined previously for MST1.[24] Finally, we discuss how these data help us understand the mechanism of action of Nore1.

MATERIALS AND METHODS

Cloning, Expression, and Purification. Murine construct Nore1A-370-413 was cloned in a pGEX-4T expression vector (GE Healthcare, Freiburg, Germany) and expressed as a recombinant GST fusion protein in *Escherichia coli* strain BL21 DE3 according to the manufacturer's recommendations. The disruption of the cells was achieved by ultrasonication for 10 min on ice. After the lysate had been cleared by centrifugation at 4 °C, the supernatant was then applied to a GST affinity chromatography column with glutathione (GSH) Sepharose beads (GE Healthcare). The column was washed extensively with buffer. The GST−Nore1-SARAH fusion protein was cleaved with thrombin, resulting in an N-terminal G-S extension of Nore1-370-413. This was done on the column at 4 °C overnight. The eluted Nore1-SARAH protein was concentrated using Vivaspin centrifugal concentrators (Sartorius AG, Goettingen, Germany). The protein was further purified by gel filtration chromatography using a Superdex 75 column (GE Healthcare), concentrated again, and shock-frozen in liquid nitrogen. The protein concentrations were measured by the Bradford assay[26] using bovine serum albumin as a reference protein.

Crystallization. At 18 °C, murine Nore1-SARAH (comprising Nore1 residues 370−413 with G and S at the N-terminus) crystallized at a concentration of 17.8 mg/mL in a solution containing 25−26% (v/v) PEG 400, 100 mM sodium acetate (pH 4.6), and 45−50 mM cadmium chloride. Under these conditions, Nore1-SARAH formed crystals with dimensions of 150 μm × 120 μm × 30 μm. For phasing, the Nore1-SARAH L379M mutant was crystallized as a selenomethionine variant at a concentration of 10 mg/mL in a solution containing 28−30% (v/v) PEG 400, 100 mM sodium acetate (pH 4.6), 50−55 mM cadmium chloride, and 6% dioxane at 18 °C. Crystals typically grew to dimensions of approximately 150 μm × 60 μm × 30 μm. Wild-type Nore1-SARAH crystallizes in space group $C222_1$ and the selenomethionine-substituted Nore1-SARAH L379M mutant in space group $I222$. For cryoprotection, crystals were briefly dipped into paraffin oil before being shock-frozen in liquid nitrogen. In the case of the selenomethionine crystals, the PEG 400 already present in the mother liquor was sufficient for cryoprotection.

Structure Solution. Oscillation data at 100 K were collected at the European Synchrotron Radiation Facility (Grenoble, France) on beamlines ID14.4 (Nore-SARAH) and ID29 (Nore1-SARAH L379SeMet). Data were processed and scaled using the XDS program suite[27] and the automatic processing package XIA2.[28] The resulting statistics are listed in Table 1. The structure of the Nore1-SARAH L379SeMet variant was determined by the SAD method, using SOLVE.[30] A preliminary model of the antiparallel homodimer was then used for molecular replacement of the Nore1-SARAH data set, using AMORE.[31] The Nore1-SARAH model was iteratively improved using CNS[32] or Refmac5[33] for automated refinement and Coot[34] or O[35] for manual rebuilding. Phenix.refine[36] was used in the final rounds of refinement. In the final model, the last five residues were not modeled because of missing density in both chains present in the asymmetric unit. The starting glycine was omitted from chain A. Three residues were modeled with alternating conformations (Q389 in chain A and R398 and R406 in chain B). Three cadmium ions were identified because of strong difference density and verified by peaks in anomalous difference maps. In addition, 88 water molecules are present in the final structure. Refinement statistics are listed in Table 1. Coordinates have been deposited in the Protein Data Bank (PDB) as entry 2YMY.

Circular Dichroism (CD). Far-UV (190−250 nm) CD spectra of Nore1-SARAH were recorded with a JASCO J-715 spectropolarimeter in 20 mM phosphate buffer (pH 7.5) and 100 mM NaCl. The following protein concentrations were used for K_D determination: 5, 10, 20, 40, 60, 80, and 100 μM. The concentrations used for thermal denaturation were 5, 10, and

Table 1. Data Collection and Refinement Statistics[a]

	Nore-SARAH L379SeMet	Nore-SARAH
PDB entry		2YMY
beamline	ESRF ID29	ESRF ID14.4
resolution (Å)	40.2−1.55 (1.59−1.55)	42−1.69 (1.73−1.69)
cell parameters		
a, *b*, *c* (Å)	46.10, 69.80, 70.80	70.82, 84.41, 39.24
α, *β*, *γ* (deg)	90, 90, 90	90, 90, 90
space group	*I*222	$C222_1$
wavelength	0.9792	0.9393
completeness (%)	97.7 (98.7)	99.3 (95.4)
multiplicity	3.5 (3.5)	6.4 (4.4)
average $I/\sigma I$	15.4 (4.0)	16.3 (2.4)
R_{sym} (%)	4.7 (26.2)	6.8 (76.4)
R_{meas} (%)[b]	5.6 (30.8)	7.4 (86.8)
$R_{mergedF}/R_{pim}$ (%)[b]	7.0 (33.0)	2.9 (40.1)
figure of merit[c]	0.33 overall	
Refinement		
resolution (Å)		42−1.69
R_{cryst} (%)		19.4
R_{free} (%)[d]		23.5
no. of atoms		
protein		817
cadmium		3
water		88
average *B* factor (Å^2)		28.8
root-mean-square deviation from ideality		
bonds (Å)		0.013
angles (deg)		1.406

[a]Data in parentheses represent values in the highest-resolution bin. [b]For the definition of R_{meas} and $R_{mergedF}$, see ref 29. [c]Calculated with SOLVE. [d]R_{free} calculated from 5% of data omitted from refinement.

15 μM. The scans were performed in a 1 or 2 mm path length, rectangular quartz cuvette. For thermal denaturation, data points were taken at 222 nm, in 5 °C intervals, with a 1 min equilibration time at each temperature and a heating rate of 1 °C/min. For 5 μM Nore1-SARAH, the spectrum at each temperature was also recorded. The spectra were recorded at a bandwidth of 1 nm and a scan rate of 50 nm/min. All measurements were an average of three consecutive scans. The buffer scans were accumulated under the same conditions and subtracted from the protein spectra before further analysis.

Isothermal Titration Calorimetry (ITC). The energetics of Nore1-SARAH dissociation and the K_D were probed by ITC, using a MicroCal ITC_{200} instrument. The solution containing 500 μM protein was titrated from the syringe into the cell (200 μL) containing only the buffer (the same buffer as for the CD measurements). The injection volume was 2 μL and the time between the injections 3 min. Thus, the protein was predominantly dimeric in the syringe, and it was diluted to concentrations at which it was predominantly monomeric. The buffers were filtered, degassed, and equilibrated at the desired temperature. The experimental points were fit with a dimer dissociation model kindly provided by A. Cooper.

RESULTS

Nore1-SARAH Forms an Antiparallel Left-Handed Homodimeric Coiled Coil. The crystal structure of Nore1-SARAH reveals that it forms an antiparallel left-handed

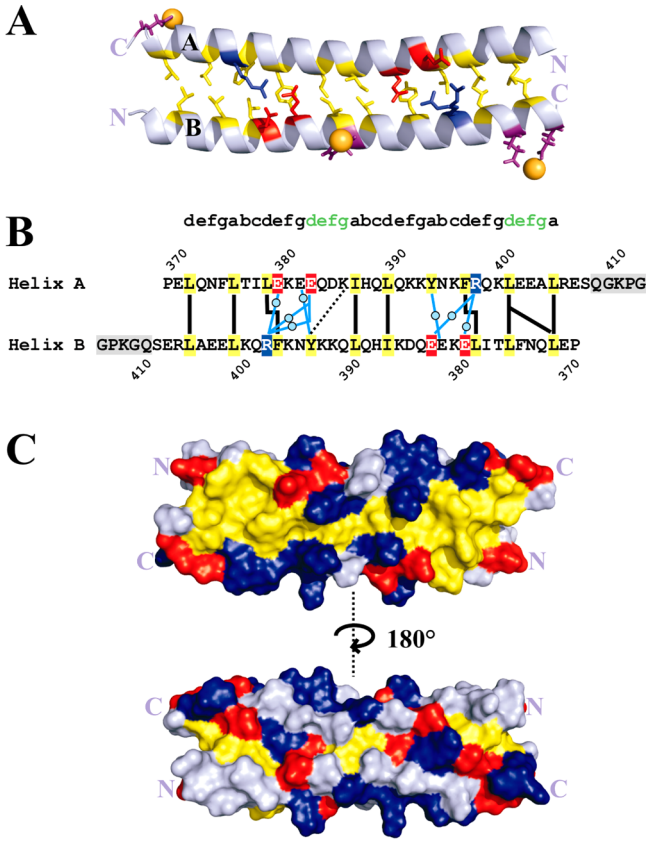

Figure 1. (A) Cartoon and stick representation of the crystal structure of murine Nore1-SARAH and (B) schematic depiction of residues mediating interhelical interactions. The stutters are highlighted in green letters (see the text). The interhelical interactions of hydrophobic and charged residues are depicted as black solid and dotted lines, respectively. Water molecules involved in interhelical interactions are depicted as blue filled circles and water-mediated polar interactions as cyan lines. Cadmium ions (depicted as orange spheres) mediate lattice contacts by coordinating residues E407 (helix A), H388 (helix B), E403 (helix B), and E407 (helix B); these residues are colored purple. Residues highlighted with a gray background (B) could not be mapped and are therefore not visible in panel A. The recombinant construct Nore1-SARAH is N-terminally extended by a G and S residue, not shown in panel B. (C) Two alternative views of Nore1-SARAH. The residues (A) and surfaces (C) are highlighted by different colors; hydrophobic, negative, positive, and remaining residues are colored yellow, red, dark blue, and light blue, respectively. Note that the orientation of Nore1-SARAH in panel A is not the same as in panels B and C (top view). This was necessary to better visualize charged residues involved in interhelical interactions. In addition, residue R398 of helix B has two alternative conformations.

homodimer with characteristics of coiled coils (Figure 1A). The last five C-terminal amino acid residues could not be mapped in the crystal structure and therefore seem to be very flexible. This flexibility is also predicted by programs like Jpred.[37] The most outstanding property of coiled coils is a seven-residue sequence (heptad) repeat, the positions of which are labeled as **a**−**g**. Positions **b**, **c**, and **e**−**g** are usually occupied by polar and charged residues, whereas positions **a** and **d** are occupied by hydrophobic ones that form the core of the helix bundle. However, the structure of Nore1-SARAH shows some deviations from an ideal coiled coil. The heptad register of the Nore1-SARAH dimer is interrupted by two stutters (residues 383−386 and 401−404) (Figure 1B). Stutters are insertions

dx.doi.org/10.1021/bi3014642 | *Biochemistry* 2013, 52, 1045−1054

Table 2. Comparison of the Primary Structures of Different SARAH Domains[a]

	Nore1	Rassf1	Rassf2	Rassf3	Rassf4	Rassf6	MST1	MST2	WW45
Nore1		76	63	87	58	61	58	58	50
Rassf1	50		66	76	50	53	50	53	45
Rassf2	29	32		66	79	68	47	53	47
Rassf3	63	53	37		55	54	62	63	47
Rassf4	26	26	58	26		66	47	47	63
Rassf6	26	24	32	18	34		50	50	50
MST1	26	34	21	24	26	24		92	53
MST2	26	32	24	37	26	21	74		50
WW45	24	24	18	26	37	21	29	24	

[a]The top half shows sequence similarities and the bottom half sequence identities. For the alignments, Nore1-370-407 was taken as a reference. This segment corresponds to the helical region of the SARAH domain.

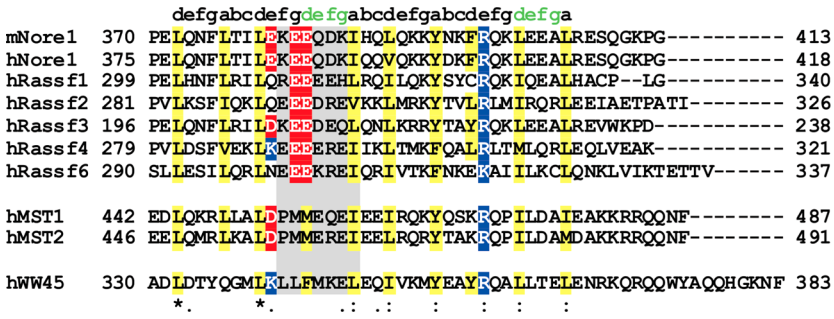

Figure 2. Comparison of the heptad repeats of murine Nore1A-SARAH with those of other human proteins. The interacting residues are highlighted in different colors; hydrophobic, negative, and positive residues are colored yellow, red, and dark blue, respectively. The two stutters are indicated by green letters. A gray background highlights the cluster consisting mainly of charged residues. Note that human Nore1A-SARAH differs from murine Nore1A-SARAH at only three positions: H388 → Q393, L390 → V395, and N398 → D400 (mNore1 → hNore1). Asterisks, colons, and periods indicate positions with fully conserved residues, conservation between residues of strongly similar physicochemical properties, and conservation between residues of moderately similar properties, respectively. The sequence alignment was performed with ClustalW2.[28]

consisting of four residues that locally decrease the level of supercoiling by forcing residues at position **a** to the center of the core (resulting in a geometry called an **x** layer) and residues at position **d** out of the center (resulting in a geometry called a **da** layer).[38] Obviously, this is one reason why the Nore1-SARAH dimer is supercoiled to only a small degree. Moreover, one of the **d** positions is occupied by the charged residue E383, and not by a hydrophobic one, as anticipated. Residues E380 and E383 form polar contacts to R398 from the other chain involving bridging water molecules (Figure 1A,B). Additional polar contacts are formed at the dimer interface by Y394 with E382 and K386. Thus, hydrophobic residues, ionic interactions, and water-mediated ionic interactions build the interhelical interface within the Nore1-SARAH dimer. The interhelical ionic interactions are important for the alignment preference (parallel vs antiparallel) and contribute to the stability of coiled coils.[39] A parallel orientation of the Nore1-SARAH dimer would lead to a destabilization of the dimer by repulsive electrostatic interactions caused by the proximity of amino acids with the same charge. As mentioned in Materials and Methods, Nore1-SARAH was crystallized in the presence of 45−50 mM cadmium chloride. The three cadmium ions present in the crystal structure of Nore1-SARAH mediate lattice contacts by chelating residues E407 (helix A) and H388, E403, and E407 (all in helix B) (Figure 1A). Neither these residues nor the cadmium ions are part of the network mediating interhelical interactions between helices A and B, so the dimer is not stabilized by divalent cadmium ions.

Interestingly, at one side within the Nore1-SARAH dimer, hydrophobic residues form a continuous patch, whereas charged and polar residues occupy almost the entire remaining surface (Figure 1C). The solvent accessible hydrophobic patch is composed partly by residues mediating interhelical interactions and partly by hydrophobic residues that do not contribute to the interhelical interaction. Possibly, this hydrophobic patch is solvent-exposed only within the Nore1-SARAH dimer but not within the full-length Nore1 dimer. Thus, other domains of Nore1 might shield this hydrophobic patch.

Structural Biological Evidence of the SARAH Domain as a Dimerization Domain. By comparing the primary structure of the SARAH domain of Nore1 (residues 370−407) with that of other proteins, we can observe a moderate to high level of sequence identity and sequence similarity (Table 2), respectively. In particular, Rassf1- and Rassf3-SARAH show very high levels of sequence similarity (according to the Gonnet PAM 250 matrix)[40] with Nore1-SARAH. The heptad repeat arrangement of Nore1-SARAH with two stutters is conserved at corresponding positions among all other SARAH domains (Figure 2). Intriguingly, like Nore1-SARAH, none of the heptad repeats of these proteins represent the very C-terminal end of the SARAH domains; instead, the heptad repeats are C-terminally followed by 6−18 additional residues (Figure 2). A remarkable feature of the SARAH domains of the Rassf family is the existence of a highly charged segment being approximately seven residues long, mainly composed of E and D residues, and a few K residues (Figure 2). The water-mediated interhelical ionic interactions via residues R398, E380, and E383, as mentioned above, are located in this cluster. The corresponding segments in hMST1 and -2 and hWW45 contain

dx.doi.org/10.1021/bi3014642 | *Biochemistry* 2013, 52, 1045−1054

fewer charged residues. The occurrence of the same heptad pattern with two stutters within the SARAH domains of all other proteins suggests that they have a structure very similar to that of Nore1-SARAH. This point of view is supported by the nuclear magnetic resonance (NMR) structure of MST1-SARAH,[25] which has a very similar heptad pattern interrupted by two stutters, too. Similar to Nore1-SARAH, MST1-SARAH also has a small degree of supercoiling. The conservation of the heptad register with two stutters within the SARAH domains of Rassf1−4, Rassf6, MST2, and WW45 suggests that they are supercoiled to a small degree, too (Figure 2).

Additionally, the SWISS-MODEL server for comparative modeling of three-dimensional protein structures was used to model the structures of Rassf1 and Rassf3 as they have very high levels of sequence identity and similarity to Nore1-SARAH (Table 2). The reliability of SWISS-MODEL was evaluated by Schwede et al. using 1200 protein sequences with known structures; 79% of the models (50−59% identical to the sequence of the template) have C_α positions deviating by less than 0.3 nm compared to those of their crystal structures.[41] Nevertheless, to demonstrate the accuracy of the Rassf1-SARAH and Rassf3-SARAH models obtained, we also compared them with the NMR structure of MST1-SARAH[25] (PDB entry 2jo8) (Figure 3). There is very good similarity

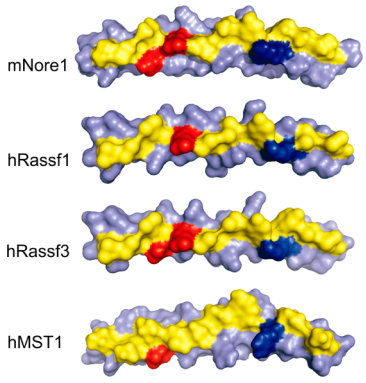

Figure 3. Comparison of the binding interfaces of the X-ray structure of Nore1A-SARAH and the NMR structure of MST1-SARAH (PDB entry 2jo8)[25] with those of Rassf1-SARAH and Rassf3-SARAH generated by SWISS-MODEL. For the sake of clarity, only one subunit of the homodimer is shown. The locations of the interacting residues are indicated by different colors; hydrophobic, negative, and positive residues are colored yellow, red, and dark blue, respectively.

between the predicted structures of the Rassf1-SARAH and Rassf3-SARAH models and the crystal structure of Nore1-SARAH. The structures of the Rassf1-SARAH and Rassf3-SARAH models are also very similar to the NMR structure of MST1-SARAH, and the locations of interhelical interacting residues are in very good agreement. This becomes more obvious upon comparison of the locations of charged residues at the interface of the models with those of the structures of Nore1-SARAH and MST1-SARAH (Figure 3).

Thermodynamic Stability of Nore1-SARAH. We have previously investigated the thermodynamic stability of the dimer and monomer of the MST1-SARAH domain.[24] We have found that the dimer is mainly stabilized by the contacts at the interface and that the monomer undergoes association-dependent folding. We wanted to see if Nore1-SARAH follows the same behavior, so we used far-UV CD spectroscopy and ITC to measure the unfolding and the dissociation of the Nore1 homodimer.

First, the effect of increasing protein concentrations on the CD spectra was investigated. The mean residue molar ellipticity, $[\Theta]_{MRW}$, of Nore1-SARAH displayed a concentration dependence as shown in Figure 4A. The ratio of ellipticity,

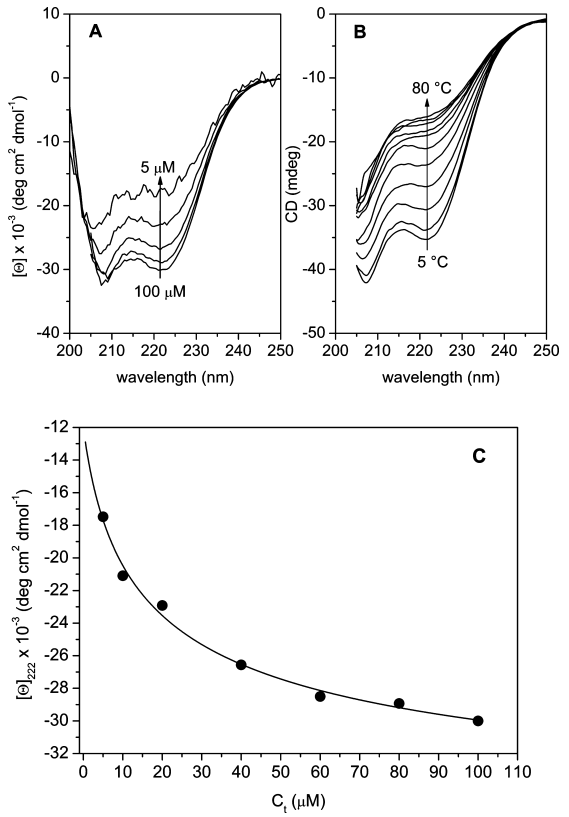

Figure 4. (A) Concentration dependence of the far-UV spectrum (molar residue ellipticity) for Nore1-SARAH at 37 °C. The concentrations of Nore1-SARAH solutions were varied between 5 and 100 μM. For the sake of clarity, only the following concentrations are shown: 5, 20, 40, 80, and 100 μM. (B) Far-UV CD spectra as a function of temperature of 5 μM Nore1-SARAH in 20 mM sodium phosphate buffer (pH 7.5) with 100 mM NaCl. (C) Molar residual ellipticity of Nore1-SARAH at 222 nm as a function of total protein concentration at 37 °C. The solid curve represents the fit according to eq 1.

$\Theta_{222}/\Theta_{208}$, is just 0.78 at 5 μM and reaches 1 at the maximal concentration used in this study (100 μM). It should be noted that this ratio is an indication of the degree of supercoiling: generally, typical coiled-coil proteins have a ratio of >1.

As the SARAH domain of Nore1 tends to further aggregate in the absence of salts and with increasing concentrations, the thermal unfolding was monitored in the presence of 100 mM NaCl, so the spectra were noisy below 205 nm. As a consequence, no information could be extracted from this region.

From the concentration dependence of the molar ellipticity (Θ) at 222 nm (Figure 4A,C), a K_D of 28 μM was obtained at 37 °C, by fitting with the following equation (Figure 4C):

$$\Theta_{obs} = \Theta_D + (\Theta_N - \Theta_D)\frac{4C_t + K_D - \sqrt{K_D^2 + 8C_tK_D}}{4C_t} \quad (1)$$

dx.doi.org/10.1021/bi3014642 | Biochemistry 2013, 52, 1045−1054

where Θ_{obs} is the observed ellipticity at 222 nm, Θ_N and Θ_D represent the signal intensities of the native and dissociated protein, respectively, K_D is the dissociation constant, and C_t is the total protein concentration. The following values were obtained from the fit: $\Theta_N = -38000 \pm 1900$ deg cm^2 dmol^{-1}, $\Theta_D = -12000 \pm 2440$ deg cm^2 dmol^{-1}, and $K_D = 28 \pm 15$ μM.

Figure 4B displays the spectra for thermal unfolding of 5 μM protein with an increase in temperature from 5 to 80 °C. The unfolding was more than 90% reversible; therefore, the process was considered in thermodynamic equilibrium, and thermodynamic analysis was applied. Using the following equation, the fraction of folded protein was calculated from the ellipticity at 222 nm measured for each temperature:

$$f_N = \frac{\Theta_{obs} - (\Theta_U + m_U T)}{\Theta_N + m_N T - (\Theta_U + m_U T)} \quad (2)$$

where Θ_{obs} is the observed ellipticity, Θ_N and Θ_U represent the signal intensities of the native and unfolded protein, respectively, and m_N and m_U are the pre- and post-transition slopes, respectively. The α-helical content of Nore1-SARAH at the starting temperature (5 °C) is 85%, and the value is still 30% at the final temperature (80 °C).

Figure 5A shows the thermal transition of Nore1-SARAH at three different concentrations (5, 10, and 15 μM) as a function of temperature. The transition was found to be cooperative and to shift to higher temperatures with increasing protein concentrations; hence, it was fit by a dimer−monomer two-state equation:

$$f_N = \frac{4K_F C_t + 1 - (8K_F C_t + 1)^{1/2}}{4K_F C_t} \quad (3)$$

with

$$K_F = \exp\left[\frac{\Delta H_{vH}}{RT}\left(1 - \frac{T}{T_m}\right) - \frac{\Delta C_p}{RT}\left(T_m - T + T \ln \frac{T}{T_m}\right) - \ln C_t\right]$$

where K_F is the folding constant, from which ΔH_{vH} (van't Hoff enthalpy) and T_m (melting temperature) are obtained.[42] The change in heat capacity (ΔC_p) was initially set to zero.[43] The resulting thermodynamic parameters are listed in Table 3. The reciprocal of T_m was plotted against the natural logarithm of the total protein concentration, C_t (Figure 5B), and fit using a derived van't Hoff equation, valid for a denaturation model involving a dimer to monomer dissociation:[44]

$$\frac{1}{T_m} = -\frac{R}{\Delta H_{conc}} \ln C_t + \frac{\Delta S_{conc}}{\Delta H_{conc}} \quad (4)$$

The enthalpy value (ΔH_{conc}) obtained from Figure 5B is 50 ± 2 kcal (mol of cooperative dimer)$^{-1}$, and the entropy of unfolding (ΔS_{conc}) is 139 ± 10 cal (mol of cooperative dimer)$^{-1}$ K^{-1}.

The Gibbs energy of unfolding (ΔG°_U) at different temperatures around the melting temperature of Nore1-SARAH was calculated from the folded and unfolded fractions, considering a dimer−monomer two-state equilibrium.[42] Figure 6A shows the plot of ΔG°_U for Nore1-SARAH as a function of temperature and the fit using the following equation:

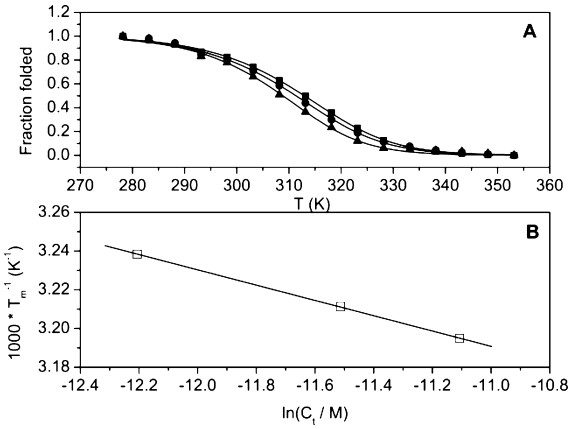

Figure 5. (A) Protein concentration dependence of the thermal denaturation of Nore1-SARAH probed by far-UV CD spectroscopy. The concentrations were 5 (▲), 10 (●), and 15 μM (■). The lines represent the best fits according to eq 3. (B) Dependence of T_m on the total monomer concentration, according to the dimer−monomer dissociation model. The line represents the fit to the experimental data using eq 4.

Table 3. Thermodynamic Parameters of the Thermal Unfolding of Nore1-SARAH from the Fit of the Individual Transitions

concn[a] (μM)	T_m (K)	ΔH_{vH} (kcal mol^{-1})
5	308.8 ± 0.1	35 ± 1
10	311.4 ± 0.1	33 ± 1
15	313.0 ± 0.1	33 ± 1

[a]Concentration calculated with the molecular mass of the monomer.

$$\Delta G^\circ_U = \Delta H_1 - \frac{T}{T_1}(\Delta H_1 - \Delta G^\circ_{U1}) + \Delta C_p\left[T - T_1 - T \ln\left(\frac{T}{T_1}\right)\right] \quad (5)$$

where ΔG°_{U1} is the unfolding Gibbs energy at reference temperature T_1, ΔH_1 is the enthalpy of unfolding at T_1, and ΔC_p values are obtained from the fit. It has to be emphasized that in the case of dimer−monomer two-state unfolding and dissociation, the Gibbs energy is not 0 (as in case of monomer two-state unfolding) but equals $-RT_m \ln C_t$ at T_m, where C_t is the total protein concentration.[43] The values calculated for different concentrations were similar, and the fit (with ΔG°_{U1} = 7.34 kcal mol^{-1} and T_1 = 313.15 K) gave a ΔH_1 (29.5 ± 1 kcal mol^{-1}) similar to the one obtained from direct analysis of thermal denaturation. A value of 0.57 ± 0.13 kcal mol^{-1} °C^{-1} was obtained for ΔC_p. At 20 °C, ΔG°_U is 8.4 kcal mol^{-1}. At this temperature, the corresponding unfolding constant, K_U, from the folded dimer to the unfolded monomer, is 0.5 μM. At 37 °C, ΔG°_U is 7.55 kcal mol^{-1} (K_U = 5 μM).

In addition, the thermodynamics of Nore1-SARAH dissociation was investigated using ITC, at two temperatures, 20 and 37 °C. Figure 7A shows the dilution experiment and the corresponding isotherm at 37 °C. A K_D (25.0 ± 2.2 μM) similar to that from CD measurements was obtained (at 37 °C). The thermodynamic parameters for both temperatures are listed in Table 4 and, for better visualization, shown in Figure 7B.

There are several interesting observations concerning the dissociation of Nore1-SARAH. First, the entropy difference is

dx.doi.org/10.1021/bi3014642 | Biochemistry 2013, 52, 1045−1054

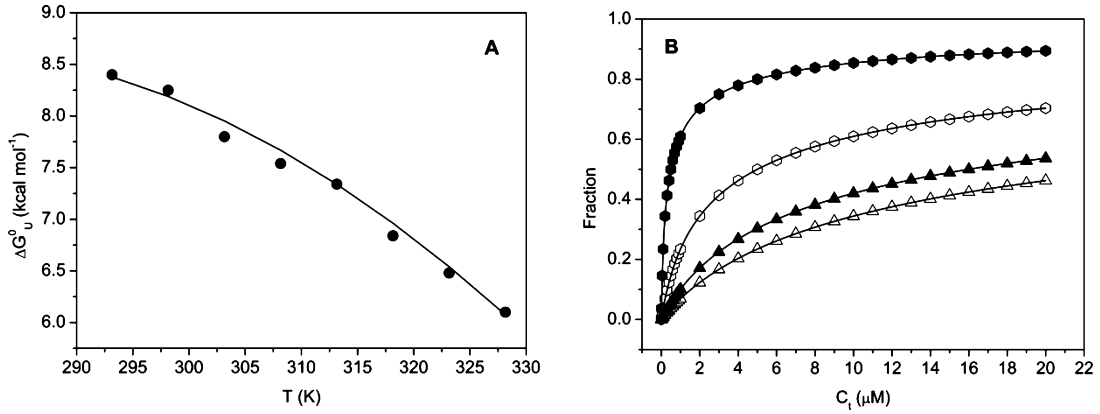

Figure 6. (A) Gibbs energy of unfolding (ΔG°_U) (thermodynamic stability) of Nore1-SARAH as a function of temperature determined by CD spectroscopic measurements under thermal denaturation conditions. The solid line represents the fit using eq 5 (see the text). (B) Fraction of folded protein (circles, measured from thermal denaturation) and associated protein (triangles, measured from dilution experiments) at 20 °C (filled symbols) and 37 °C (empty symbols).

negative at 20 °C, implying that the dissociation is both enthalpically and entropically unfavored at this temperature. On the other hand, at 37 °C, the process is enthalpically unfavored but entropically favored. The enthalpy and entropy compensate each other, resulting in a low and practically constant value for the Gibbs energy of dissociation (ΔG_{diss}). In addition, it can be also concluded that the Nore1-SARAH dimer has its maximal stability within this temperature range (where ΔS_{diss} is 0).

A comparison between the free energy of unfolding and the Gibbs energy of dissociation (ΔG_{diss}) was performed at 20 and 37 °C to confirm that the dissociation is accompanied by unfolding at the physiologically relevant temperature. The difference between the Gibbs energy of unfolding and that of dissociation (Table 3) is 1.97 kcal mol^{-1} at 20 °C and 1.02 kcal mol^{-1} at 37 °C. These values represent the stabilities of the two monomers after the dimer dissociation, which implies that the stability of one monomer is 1 kcal mol^{-1} at 20 °C and 0.5 kcal mol^{-1} at 37 °C. From the free energies of unfolding and dissociation, the fraction of folded protein and that of associated protein were calculated, respectively, as depicted in Figure 6B.

DISCUSSION

Nore1-SARAH crystallizes as an antiparallel homodimeric coiled coil (Figure 1). The Nore1-SARAH homodimer is not an ideal coiled coil, as its heptad register is interrupted by two stutters that cause a decrease in the degree of supercoiling. The modeled structures of Rassf1-SARAH and Rassf3-SARAH indicate that they also form homodimers, as the residues mediating the interhelical interactions form a patch very similar to Nore1-SARAH (to the NMR structure of MST1-SARAH, too) (Figure 3). The heptad pattern observed in Nore1-SARAH and in MST1-SARAH can also be observed in the SARAH domains of Rassf1−4, Rassf6, MST2, and WW45 (Figure 2). The residues at positions **a** and **d** of the heptad repeats dominate the overall structure of coiled coils.[38] Moreover, the presence of hydrophobic residues at positions **e** and **g** can specify the formation of antiparallel homotetramers,[45] but this is only true in cases where positions **e** and **g** are almost completely occupied by hydrophobic residues. In such tetramers, the residues at positions **a**, **d**, **e**, and **g** are buried within the hydrophobic core of the helix bundle. However, positions **e** and **g** within the heptad repeat, not only of Nore1-SARAH but also within the SARAH domains of all other proteins, are rarely occupied by hydrophobic residues. Therefore, it seems to be very unlikely that the SARAH domains of the other proteins form higher-order oligomers as had been assumed previously.[23]

An important observation concerning the dimer interface of Nore1-SARAH is the occurrence of stabilizing (water-mediated) interchain polar interactions formed by residues E380, E383 with R398, and E382 with Y394 (Figure 1B). Additionally, there is a polar contact between Y394 (helix B) and K386 (helix A). According to studies by Monera et al., such interchain interactions specify the orientation of coiled coils.[39] Apart from hRassf6, R398 is conserved in all other SARAH domains and seems to play together with E383 an important role in this context. E382 and E383 are conserved among all Rassf family members, but not in MST1- and -2 or WW45. Y394 is conserved, apart from Rassf4 and -5 (where it is replaced with phenylalanine), in all SARAH domains. Interestingly, E383 is surrounded by many other (negatively) charged residues (Figure 2). This highly charged cluster is also present in the SARAH domains of all other Rassf family members. As this cluster is mainly composed of E and D residues, it is very likely that a parallel orientation would lead to a destabilization of the dimer by repulsive interactions. Moreover, it is possible that this cluster contributes to the heterotypic binding specificities between different SARAH domains.

The last six C-terminal amino acids of Rassf-SARAH could not be mapped and are obviously not structured. Likewise, the last seven C-terminal residues of MST1 are also flexible.[25] Furthermore, the last 6−18 C-terminal residues of other SARAH domain-containing proteins are predicted by Jpred (a secondary structure prediction software)[37] to be flexible, too. The flexibility of the C-terminal ends of the SARAH domains may enlarge the space for the search of a binding partner and, hence, facilitate the binding of interaction partners.

The NMR structure of MST1-SARAH shows that it forms an antiparallel homodimer with a heptad pattern similar to that of Nore1-SARAH.[25] As the level of sequence similarity between MST1-SARAH and MST2-SARAH is very high (93.5%), it is very probable that MST2-SARAH also forms a homodimer.

Like that of MST1-SARAH,[24] the thermal denaturation of Nore1-SARAH is concentration-dependent, the T_m increasing

dx.doi.org/10.1021/bi3014642 | *Biochemistry* 2013, 52, 1045−1054

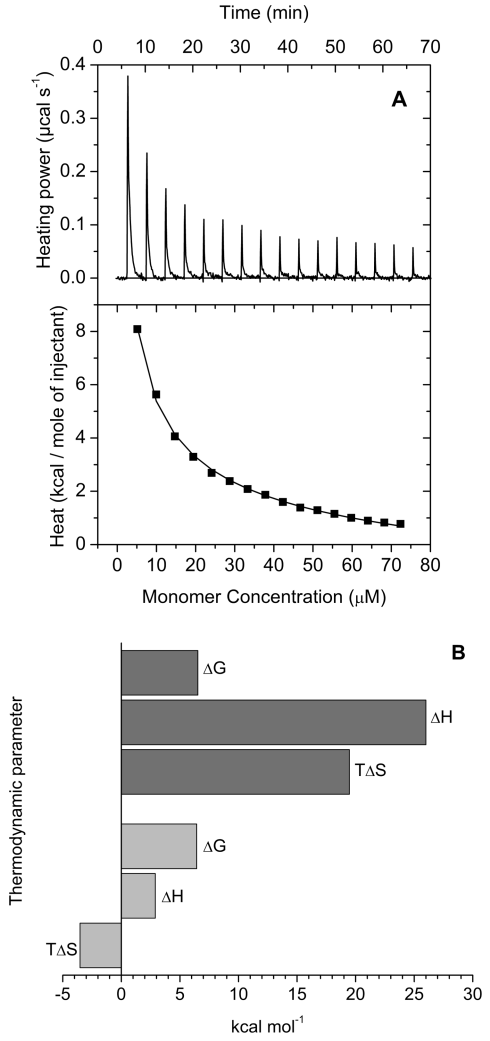

Figure 7. (A) ITC dilution experiments with Nore1-SARAH at 37 °C. The protein concentration in the syringe was 500 μM, and the injection volume was 2 μL and the cell volume 200 μL. (A) Calorimetric dilutions resulting from the titration of the Nore1-SARAH solution from the syringe into the sample cell of the ITC device (top panel). The isotherm in the bottom panel was fit by a dimer to monomer dissociation model kindly provided by A. Cooper. (B) Comparison of thermodynamic parameters at 20 (light gray) and 37 °C (dark gray).

Table 4. Thermodynamic Data for the Dissociation of Nore1-SARAH (ITC)

temp (K)	K_D[a] (μM)	ΔH_{diss}[a] (kcal mol^{-1})	ΔG_{diss} (kcal mol^{-1})	$T\Delta S_{diss}$ (kcal mol^{-1})
293	16.00 ± 1.10	2.90 ± 0.05	6.43	−3.53
310	25.00 ± 2.20	26.00 ± 0.50	6.53	19.47

[a]The errors are from each isotherm fit.

with an increase in concentration. Thus, the protein undergoes dissociation during unfolding. The unfolding transition and the linear dependency of the inverse of the T_m with the natural logarithm of the total protein concentration indicate an apparent cooperative unfolding and dissociation. Nevertheless, ΔH_{conc} is slightly higher (50 kcal mol^{-1}) than ΔH_{vH} (35 kcal mol^{-1}), implying possible intermediate states and/or incomplete dissociation. This is also sustained by the fact that there is a small difference of 1 kcal mol^{-1} between the free energy of the thermal denaturation and the free energy of dissociation at 37 °C. Thus, the dissociation does not trigger the complete unfolding of the monomer. On the other hand, the low stability (1 kcal mol^{-1}) of this intermediate state makes it undetectable during the denaturation transition. The stability of the monomer decreases faster with temperature than that of the dimer (implying interface stability), resulting in a smaller folded monomeric fraction at 37 °C than at 20 °C (Figure 6B). Also, because the Nore1-SARAH monomer is more stable than MST1-SARAH, there is a higher fraction of folded monomer intermediate during the thermal transition.

An observation has to be mentioned at this point, i.e., the relatively constant value of ΔH_{vH} with changes in protein concentration (Table 3). It could be argued that one should see an increase in this parameter with an increase in protein concentration, as for a positive heat capacity difference, one expects to see an increase in enthalpy with temperature. Nevertheless, there are some points that have to be mentioned here. First, when using a limited range of protein concentrations, one generally obtains a small shift in temperature (in our case just 4 °C). Within this range, one does not expect a large change in enthalpy (especially when the heat capacity difference is small, e.g., a ΔC_p of 0.57 ± 0.13 kcal mol^{-1} deg^{-1} would yield a maximal increase of 2−3 kcal mol^{-1}). This seems to be the case in our study as there is a linear dependence of the reciprocal transition temperature with the logarithm of the total protein concentration (expressed on a per mole basis), which implies a relatively constant enthalpy (see also ref 44) within this temperature range. A second point would be that the difference in heat capacity is approximated to be temperature-independent, within the limited temperature range studied at least. If we compare the enthalpy obtained from the plot of the Gibbs energy (29.5 kcal mol^{-1}) with that obtained from the fit of the unfolding fraction (33 kcal mol^{-1}), we can see that there is a difference of approximately 10%. This might result from the approximation of a constant ΔC_p between 290 and 330 K used when fitting the points in Figure 6A. Between 310 and 314 K, ΔC_p should not vary very much, but all the points mentioned above contribute to the results listed in Table 3. In addition, generally one does not determine ΔC_p by varying the protein concentration, but other parameters like pH.

Interestingly, the α-helical content is still 30% at the highest temperature (80 °C). This indicates that, even if the dissociation of Nore1-SARAH is accompanied by the observed unfolding, there is still substantially residual helical structure in the monomer.

Another important observation is that the Nore1-SARAH homodimer is much less stable than the MST1-SARAH homodimer and that at relatively high concentrations (5−15 μM) the protein is already approximately 70% dissociated (from which 50% unfolded) at a physiologically relevant temperature (37 °C). This is explained by the presence of water molecules at the interface of the Nore1-SARAH homodimer within the negatively charged cluster mentioned above (Figures 1B and 2). Some of the water molecules even mediate ionic interactions, leading to less packing of the residues and a smaller and less hydrophobic interface surface area. This information is highly important as, depending on the total protein concentration expressed in the cell, the protein will be predominantly dimeric or predominantly monomeric, states that affect its activity. Even though other factors could influence the interaction with its partners, the level of expression of Nore1-SARAH and other SARAH-containing proteins has to

dx.doi.org/10.1021/bi3014642 | Biochemistry 2013, 52, 1045−1054

be taken into consideration: an overly high concentration could inhibit the protein by locking it in a homodimeric state. The high K_D of the Nore1-SARAH homodimer at 37 °C could signify that Nore1 also has to be in a monomeric state. It would be interesting to quantify the level of expression under different conditions and responses of the cell.

In relation to this, it is important to draw attention to the large difference between the dissociation enthalpy at 20 °C and that at 37 °C. This most likely comes from a higher degree of unfolding at higher temperatures. Unfortunately, it is not easy to separate very clearly these contributions, as we could not measure the monomer unfolding separately with our techniques. Thus, all the thermodynamic parameters have contributions from both unfolding and dissociation. At this point, we do not know exactly how the monomer stability varies with temperature, but we will investigate this in a future study.

The low affinity of the Nore1-SARAH homodimer and the high affinity and the long lifetime of the Ras−Nore1 complex[15] are in agreement with Nore1 acting mainly as an adaptor protein that can localize MST1 and -2 at specific sites and couple them with diverse activating inputs.[7] Further studies of how the different affinities and other factors influence the equilibrium between the homodimers and the heterodimers will improve our understanding of the mechanism of Ras-mediated apoptosis. Also, it will be interesting to see the effect that different salt concentrations have on the affinities and specificities of the different homo- and heterodimers, and this will be the subject of a future study. In summary, our results support our conclusion that the SARAH domain is a helical module mediating dimeric interactions with proteins from the Rassf as well as the MST family.

AUTHOR INFORMATION

Corresponding Author

*Telephone: +49 (0)234 32-24173. Fax: +49 (0)234 32-14785. E-mail: chr.herrmann@rub.de.

Present Address

[⊥]School of Chemistry, University of St. Andrews, St. Andrews, U.K.

Author Contributions

C.M., D.C.A., and E.H. contributed equally to this work.

Funding

This work was financially supported by Deutsche Forschungsgemeinschaft SFB 642 and the Marie Curie EU Project INTCHEM (MEST-CT-2005-020681; fellowship for D.C.A.).

Notes

The authors declare no competing financial interest.

ACKNOWLEDGMENTS

We kindly thank Prof. Dr. Alan Cooper from the University of Glasgow (Glasgow, U.K.) for providing the dimer dissociation model used for our ITC experiments. Thanks are also due to the beamline staff at the European Synchroton Radiation Facility, beamlines ID14.4 and ID29. We also acknowledge Dr. Ingrid Vetter for help during data processing and structure solution.

REFERENCES

(1) Vos, M. D., Ellis, C. A., Elam, C., Ulku, A. S., Taylor, B. J., and Clark, G. J. (2003) RASSF2 is a novel K-Ras-specific effector and potential tumor suppressor. *J. Biol. Chem. 278*, 28045−28051.

(2) Eckerd, K., Hesson, L., Vos, M. D., Bieche, I., Latif, F., and Clark, G. J. (2004) RASSF4/AD037 is a potential ras effector/tumor suppressor of the RASSF family. *Cancer Res. 64*, 8688−8693.

(3) Ikeda, M., Hirabayashi, S., Fujiwara, N., Mori, H., Kawata, A., Iida, J., Bao, Y., Sato, Y., Iida, T., Sugimura, H., and Hata, Y. (2007) Ras-association domain family protein 6 induces apoptosis via both caspase-dependent and caspase-independent pathways. *Exp. Cell Res. 313*, 1484−1495.

(4) Allen, N. P., Donninger, H., Vos, M. D., Eckfeld, K., Hesson, L., Gordon, L., Birrer, M. J., Latif, F., and Clark, G. J. (2007) RASSF6 is a novel member of the RASSF family of tumor suppressors. *Oncogene 26*, 6203−6211.

(5) Vos, M. D., Martinez, A., Ellis, C. A., Vallecorsa, T., and Clark, G. J. (2003) The proapoptotic Ras effector Nore1 may serve as a Ras-regulated tumor suppressor in the lung. *J. Biol. Chem. 278*, 21938−21943.

(6) Khokhlatchev, A., Rabizadeh, S., Xavier, R., Nedwidek, M., Chen, T., Zhang, X. F., Seed, B., and Avruch, J. (2002) Identification of a novel Ras-regulated proapoptotic pathway. *Curr. Biol. 12*, 253−265.

(7) Praskova, M., Khoklatchev, A., Ortiz-Vega, S., and Avruch, J. (2004) Regulation of the MST1 kinase by autophosphorylation, by the growth inhibitory proteins, RASSF1 and NORE1, and by Ras. *Biochem. J. 381*, 453−462.

(8) Moshnikova, A., Frye, J., Shay, J. W., Minna, J. D., and Khokhlatchev, A. V. (2006) The growth and tumor suppressor NORE1A is a cytoskeletal protein that suppresses growth by inhibition of the ERK pathway. *J. Biol. Chem. 281*, 8143−8152.

(9) Bee, C., Moshnikova, A., Mellor, C. D., Molloy, J. E., Koryakina, Y., Stieglitz, B., Khokhlatchev, A., and Herrmann, C. (2010) Growth and tumor suppressor NORE1A is a regulatory node between Ras signaling and microtubule nucleation. *J. Biol. Chem. 285*, 16258−16266.

(10) Shivakumar, L., Minna, J., Sakamaki, T., Pestell, R., and White, M. A. (2002) The RASSF1A tumor suppressor blocks cell cycle progression and inhibits cyclin D1 accumulation. *Mol. Cell. Biol. 22*, 4309−4318.

(11) Aoyama, Y., Avruch, J., and Zhang, X. F. (2004) Nore1 inhibits tumor cell growth independent of Ras or the MST1/2 kinases. *Oncogene 23*, 3426−3433.

(12) Hesson, L., Dallol, A., Minna, J. D., Maher, E. R., and Latif, F. (2003) NORE1A, a homologue of RASSF1A tumour suppressor gene is inactivated in human cancers. *Oncogene 22*, 947−954.

(13) Katagiri, K., Imamura, M., and Kinashi, T. (2006) Spatiotemporal regulation of the kinase Mst1 by binding protein RAPL is critical for lymphocyte polarity and adhesion. *Nat. Immunol. 7*, 919−928.

(14) Fujita, H., Fukuhara, S., Sakurai, A., Yamagishi, A., Kamioka, Y., Nakaoka, Y., Masuda, M., and Mochizuki, N. (2005) Local activation of Rap1 contributes to directional vascular endothelial cell migration accompanied by extension of microtubules on which RAPL, a Rap1-associating molecule, localizes. *J. Biol. Chem. 280*, 5022−5031.

(15) Stieglitz, B., Bee, C., Schwarz, D., Yildiz, O., Moshnikova, A., Khokhlatchev, A., and Herrmann, C. (2008) Novel type of Ras effector interaction established between tumour suppressor NORE1A and Ras switch II. *EMBO J. 23*, 1995−2005.

(16) Downward, J. (2003) Targeting RAS signalling pathways in cancer therapy. *Nat. Rev. Cancer 3*, 11−22.

(17) Waldman, T., Zhang, Y., Dillehay, L., Yu, J., Kinzler, K., Vogelstein, B., and Williams, J. (1997) Cell-cycle arrest versus cell death in cancer therapy. *Nat. Med. 3*, 1034−1036.

(18) Graves, J. D., Gotoh, Y., Draves, K. E., Ambrose, D., Han, D. K. M., Wright, M., Chernoff, J., Clark, E. A., and Krebs, E. G. (1998) Caspase-mediated activation and induction of apoptosis by the mammalian Ste20-like kinase Mst1. *EMBO J. 17*, 2224−2234.

(19) Park, J., Kang, S. I., Lee, S. Y., Zhang, X. F., Kim, M. S., Beers, L. F., Lim, D. S., Avruch, J., Kim, H. S., and Lee, S. B. (2010) Tumor suppressor ras association domain family 5 (RASSF5/NORE1) mediates death receptor ligand-induced apoptosis. *J. Biol. Chem. 285*, 35029−35038.

(20) Dittfeld, C., Richter, A. M., Steinmann, K., Klagge-Ulonska, A., and Dammann, R. H. (2012) The SARAH Domain of RASSF1A and Its Tumor Suppressor Function. *Mol. Biol. Int. 2012*, 196715.
(21) Callus, B. A., Verhagen, A. M., and Vaux, D. L. (2006) Association of mammalian sterile twenty kinases, Mst1 and Mst2, with hSalvador via C-terminal coiled-coil domains, leads to its stabilization and phosphorylation. *FEBS J. 273*, 4264−4276.
(22) van der Weyden, L., and Adams, D. J. (2007) The Ras-association domain family (RASSF) members and their role in human tumourigenesis. *Biochim. Biophys. Acta 1776*, 58−85.
(23) Scheel, H., and Hofmann, K. (2003) A novel interaction motif, SARAH, connects three classes of tumor suppressor. *Curr. Biol. 13*, 899−900.
(24) Constantinescu Aruxandei, D., Makbul, C., Koturenkiene, A., Lüdemann, M. B., and Herrmann, C. (2011) Dimerization-induced folding of MST1 SARAH and the influence of the intrinsically unstructured inhibitory domain: Low thermodynamic stability of monomer. *Biochemistry 50*, 10990−11000.
(25) Hwang, E., Ryu, K. S., Paakkonen, K., Guntert, P., Cheong, H. K., Lim, D. S., Lee, J. O., Jeon, Y. H., and Cheong, C. (2007) Structural insight into dimeric interaction of the SARAH domains from Mst1 and RASSF family proteins in the apoptosis pathway. *Proc. Natl. Acad. Sci. U.S.A. 104*, 9236−9241.
(26) Bradford, M. M. (1976) A Rapid and Sensitive Method for the Quantitation of Microgram Quantities of Protein Utilizing the Principle of Protein-Dye Binding. *Anal. Biochem. 72*, 248−254.
(27) Kabsch, W. (2010) XDS. *Acta Crystallogr. D66*, 125−132.
(28) Winter, G. (2010) xia2: An expert system for macromolecular crystallography data reduction. *J. Appl. Crystallogr. 43*, 186−190.
(29) Diederichs, K., and Karplus, P. A. (1997) Improved R-factors for diffraction data analysis in macromolecular crystallography. *Nat. Struct. Biol. 4*, 269−275.
(30) Terwilliger, T. C., and Berendzen, J. (1999) Automated MAD and MIR structure solution. *Acta Crystallogr. D55*, 849−861.
(31) Navaza, J. (1994) AMoRe: An automated package for molecular replacement. *Acta Crystallogr. A50*, 157−163.
(32) Brunger, A. T., Adams, P. D., Clore, G. M., Gros, P., Grosse-Kunstleve, R. W., Jiang, J.-S., Kuszewski, J., Nilges, N., Pannu, N. S., Read, R. J., Rice, L. M., Simonson, T., and Warren, G. L. (1998) Crystallography & NMR System (CNS): A new software suite for macromolecular structure determination. *Acta Crystallogr. D54*, 905−921.
(33) Murshudov, G. N., Vagin, A., and Dodson, E. J. (1997) Refinement of Macromolecular Structures by the Maximum-Likelihood Method. *Acta Crystallogr. D53*, 240−255.
(34) Emsley, P., and Cowtan, K. (2004) Coot: Model-building tools for molecular graphics. *Acta Crystallogr. D60*, 2126−2132.
(35) Jones, T. A., Zou, J.-Y., Cowan, S. W., and Kjeldgaard, M. (1991) Improved methods for the building of protein models in electron density maps and the location of errors in these models. *Acta Crystallogr. A47*, 110−119.
(36) Adams, P. D., Afonine, P. V., Bunkóczi, G., Chen, V. B., Davis, I. W., Echols, N., Headd, J. J., Hung, L.-W., Kapral, G. J., Grosse-Kunstleve, R. W., McCoy, A. J., Moriarty, N. W., Oeffner, R., Read, R. J., Richardson, D. C., Richardson, J. S., Terwilliger, T. C., and Zwart, P. H. (2010) PHENIX: A comprehensive Python-based system for macromolecular structure solution. *Acta Crystallogr. D66*, 213−221.
(37) Cole, C., Barber, J. D., and Barton, G. J. (2008) The Jpred secondary structure prediction server. *Nucleic Acids Res. 35*, 197−201.
(38) Lupas, A. N., and Gruber, M. (2005) The structure of α-helical coiled coils. *Adv. Protein Chem. 70*, 37−78.
(39) Monera, O. D., Zhou, N. E., Kay, C. M., and Hodges, R. S. (1993) Comparison of antiparallel and parallel two-stranded α-helical coiled-coils. Design, synthesis, and characterization. *J. Biol. Chem. 268*, 19218−19227.
(40) Larkin, M. A., Blackshields, G., Brown, N. P., Chenna, R., McGettigan, P. A., McWilliam, H., Valentin, F., Wallace, I. M., Wilm, A., Lopez, R., Thompson, J. D., Gibson, T. J., and Higgins, D. G. (2007) Clustal W and Clustal X version 2.0. *Bioinformatics 23*, 2947−2948.
(41) Schwede, T., Diemand, A., Guex, N., and Peitsch, M. C. (2000) Protein structure computing in the genomic era. *Res. Microbiol. 151*, 107−112.
(42) Shriver, J. W., and Edmondson, S. P. (2009) Defining the Stability of Multimeric Proteins. In *Protein Structure, Stability, and Interactions* (Shriver, J. W., Ed.) pp 57−82, Humana Press, Totowa, NJ.
(43) Greenfield, N. J. (2006) Using circular dichroism collected as a function of temperature to determine the thermodynamics of protein unfolding and binding interactions. *Nat. Protoc. 1*, 2527−2535.
(44) Lassalle, M. W., Hinz, H.-J., Wenzel, H., Vlassi, M., Kokkinidis, M., and Cesareni, G. (1998) Dimer-to-Tetramer Transformation: Loop Excision Dramatically Alters Structure and Stability of the Rop four α-helix Bundle Protein. *J. Mol. Biol. 279*, 987−1000.
(45) Liu, J., Zheng, Q., Deng, Y., Cheng, C. S., Kallenbach, N. R., and Lu, M. (2006) A seven-helix coiled coil. *Proc. Natl. Acad. Sci. U.S.A. 103*, 15457−15462.